Terahertz intersubband absorption of GaN/ AlGaN step quantum wells grown by MOVPE on Si(111) and Si(110) substrates

A Jollivet, M Tchernycheva, V Trinité, E Frayssinet, P de Mierry, Y Cordier, F H Julien

Applied Physics Letters

Terahertz intersubband absorption of GaN/AlGaN step quantum wells grown by MOVPE on Si(111) and Si(110) substrates

Cite as: Appl. Phys. Lett. **115**, 261103 (2019); https://doi.org/10.1063/1.5129362
Submitted: 29 September 2019 . Accepted: 13 December 2019 . Published Online: 26 December 2019

A. Jollivet, M. Tchernycheva, V. Trinité, E. Frayssinet, P. De Mierry, Y. Cordier, and F. H. Julien

Applied Physics Letters ARTICLE scitation.org/journal/apl

Terahertz intersubband absorption of GaN/AlGaN step quantum wells grown by MOVPE on Si(111) and Si(110) substrates

Cite as: Appl. Phys. Lett. **115**, 261103 (2019); doi: 10.1063/1.5129362
Submitted: 29 September 2019 · Accepted: 13 December 2019 ·
Published Online: 26 December 2019

A. Jollivet,[1,a)] M. Tchernycheva,[1] V. Trinité,[2] E. Frayssinet,[3] P. De Mierry,[3] Y. Cordier,[3] and F. H. Julien[1]

AFFILIATIONS

[1]Centre de Nanosciences et de Nanotechnologies (C2N), CNRS UMR 9001, Université Paris-Sud, Université Paris-Saclay, 91120 Palaiseau, France
[2]III-V Lab, 91767 Palaiseau, France
[3]Université Côte d'Azur, CNRS, CRHEA, 06560 Valbonne, France

[a)]**Author to whom correspondence should be addressed:** arnaud.jollivet@c2n.upsaclay.fr

ABSTRACT

We demonstrate terahertz intersubband absorptions in nitride step quantum wells (SQWs) grown by metal organic vapor phase epitaxy simultaneously on two different substrate orientations [Si(111) and Si(110)]. The structure of the SQWs consists of a 3 nm thick $Al_{0.1}Ga_{0.9}N$ barrier, a 3 nm thick GaN well, and an $Al_{0.05}Ga_{0.95}N$ step barrier with various thicknesses. This structure design has been optimized to approach a flatband potential in the wells to allow for an intersubband absorption in the terahertz frequency range and to maximize the optical dipole moment. Structural characterizations prove the high quality of the samples. Intersubband absorptions at frequencies of 5.6 THz ($\lambda \approx 54\ \mu$m), 7 THz (43 μm), and 8.9 THz (34 μm) are observed at 77 K on both substrate orientations. The observed absorption frequencies are in excellent agreement with calculations accounting for the depolarization shift induced by the electron concentration in the wells.

Published by AIP Publishing. https://doi.org/10.1063/1.5129362

The terahertz (THz) spectral region is subject to increased interest thanks to a broad range of its applications such as molecular spectroscopy, medical diagnostics, security screening, or material quality control. Quantum cascade lasers (QCLs) based on intersubband (ISB) transitions are now well-established solid-state sources to cover this frequency domain.[1–4] The current technology based on GaAs/AlGaAs quantum wells (QWs) can provide a few tens-of-milliwatt power in pulsed mode and emission in the 0.85–4.6 THz spectral range. The high frequency limit of 4.6 THz is limited by the reststrahlen absorption band of GaAs, which extends from 4.6 to 12 THz. This limitation can be lifted if GaAs is replaced by GaN. Indeed, GaN offers prospects for THz quantum cascade devices operating in a much broader spectral range from 1 to 15 THz, which cannot be covered by other III–V semiconductors. The reason is the large energy of A_1 LO-phonons (92 meV) for GaN with respect to 36 meV for GaAs. In addition, it was predicted that thanks to their large LO-phonon energy, wide bandgap semiconductors such as GaN would pave the way for THz QCLs operating above room temperature.[5–7] The maximum operating temperature for GaAs QCLs reported so far is 210.5 and 129 K for pulsed and continuous wave operation, respectively, which is too low for widespread applications.[8,9] The small energy of the longitudinal optical LO phonon in GaAs hinders laser action close to room temperature because of nonradiative relaxations due to thermally activated LO-phonon emissions.

One difficulty for tuning ISB transitions to the terahertz frequency domain using GaN-based semiconductors grown along the polar c-axis is the presence of spontaneous and piezoelectric polarizations, which translates into huge internal electric fields in the epitaxial layers.[10] We have shown that by increasing the well thickness and reducing the Al content of AlGaN barrier layers, the ISB absorption wavelength could not be increased beyond 12 μm due to the quantum confinement induced by the internal field in the GaN wells.[11] Another strategy for reaching the terahertz spectral range is to make use of semipolar or nonpolar orientations or even of cubic nitrides.[12–14] However, the presence of a large density of misfit dislocations in these structures is detrimental to vertical transport devices such as QCLs. An alternate strategy is to make use of high-quality polar step-QWs, which consist of a GaN well, a low-Al content step barrier, and a higher Al content AlGaN barrier grown along the c-axis. With the right choice of the Al content in the step barrier, it is possible to emulate the conduction energy profile of a square QW. Not only the ISB oscillator strength is maximized but also the ISB transition energy is

governed by the step-barrier thickness. The first demonstration of THz ISB absorptions in step GaN QWs was achieved using plasma-assisted molecular beam epitaxy (PA-MBE) growth on Si(111) high-resistivity substrates.[15] Using the same epitaxial technique, a quantum well infrared photodetector (QWIP) based on double-step GaN/AlGaN QWs was demonstrated operating at 13 THz.[16] ISB absorption at THz frequencies has also been observed in double-step GaN/AlGaN QWs grown by PA-MBE although with a large broadening factor.[17] To summarize, today the observations of THz ISB absorptions in nitride QWs are limited to MBE-grown structures; however, the small growth rate of PA-MBE is not optimal for the elaboration of thick QCL layers requiring a large number of periods.[18]

In this paper, we report on the observation of THz ISB absorptions in GaN/AlGaN step QWs grown by metal organic vapor phase epitaxy (MOVPE), which is a technique of choice for the growth of thick structures. Two series of samples are grown at 1050 °C simultaneously on Si(111) or Si(110) high-resistivity substrates. The structures under investigation are superlattices of step-QWs, composed of a GaN well, an $Al_{0.05}Ga_{0.95}N$ step barrier, and an $Al_{0.1}Ga_{0.9}N$ barrier. The samples have been investigated using atomic force microscopy (AFM) as well as

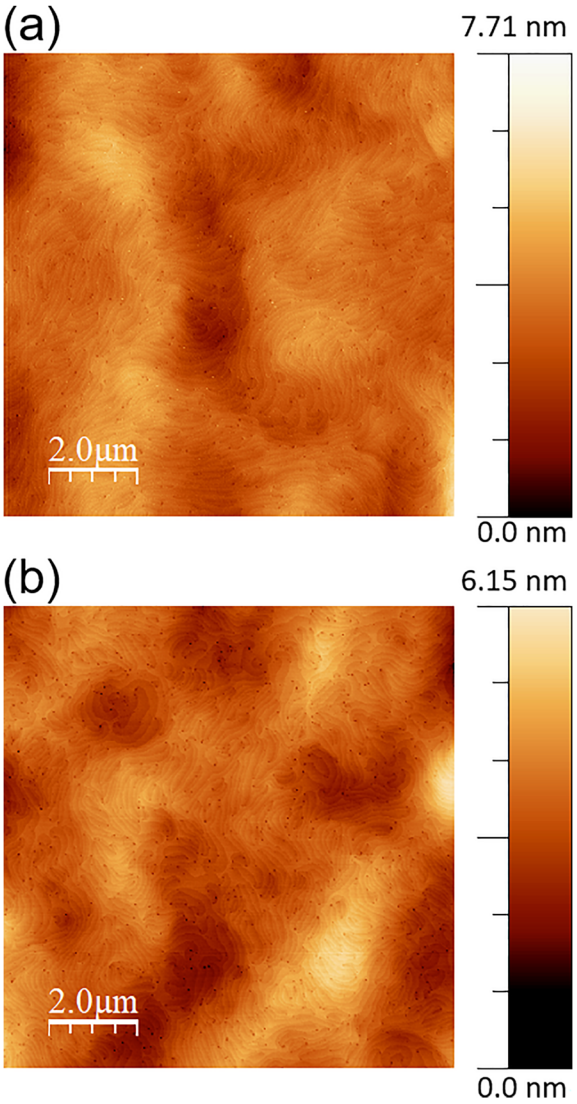

FIG. 1. AFM images ($10 \times 10\ \mu m^2$) of samples A_{111} (a) and A_{110} (b). The RMS roughness is about 0.7 nm.

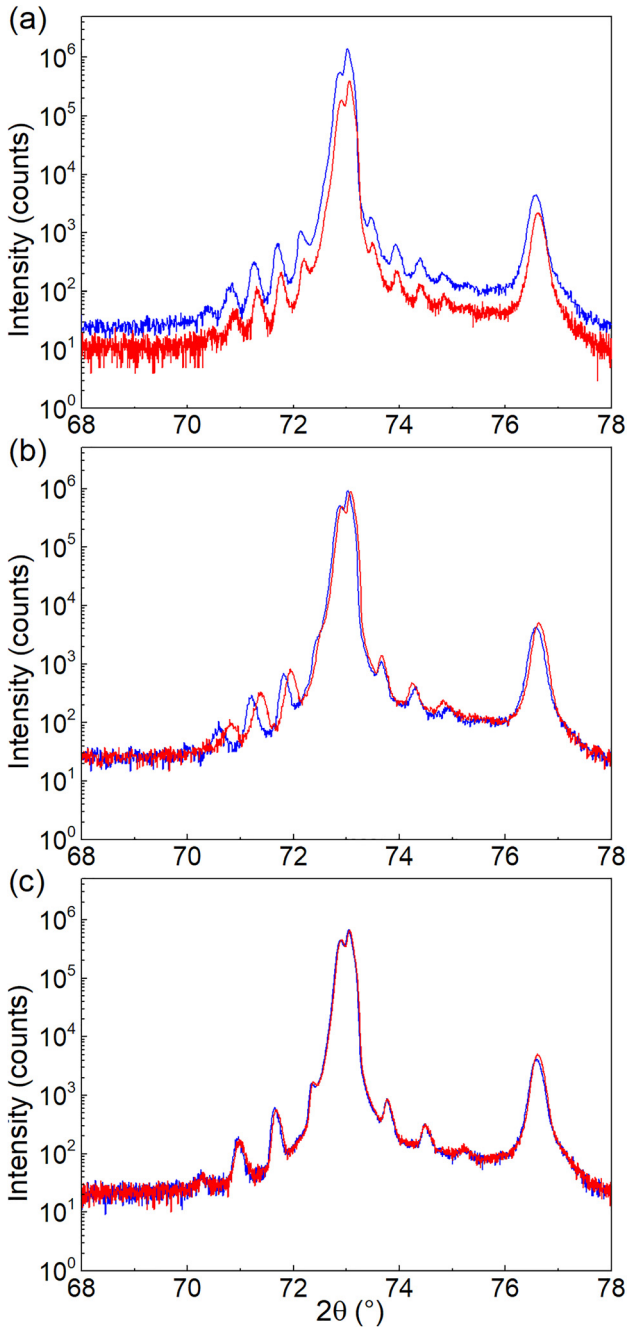

FIG. 2. High-resolution $\omega - 2\theta$ scan around the (0002) x-ray reflection of samples A, B, and C grown on Si(111) (red) and Si(110) (blue) substrates.

X-ray diffraction (XRD), secondary ion mass spectrometry (SIMS), and Fourier transform infrared (FTIR) spectroscopies. All samples reveal TM-polarized THz ISB absorption at liquid nitrogen temperature peaked at 5.6 THz, 7 THz, and 8.9 THz, respectively. The resonant ISB absorption energy is in good agreement with simulations accounting for the depolarization shift due to the electron concentration.

A series of 6 samples has been grown by MOVPE. The sample active region consists of a 40-period superlattice of step-QWs formed by a nominal 3 nm thick GaN well, an $Al_{0.05}Ga_{0.95}N$ step barrier, and a nominal 3 nm thick $Al_{0.1}Ga_{0.9}N$ spacer barrier. The nominal step barrier thickness is 15 nm, 10 nm, and 7.5 nm for samples A, B, and C, respectively. The GaN wells are n-doped with silicon. A 50 nm thick $Al_{0.05}Ga_{0.95}N$ cap layer terminates the growth. Samples labeled A_{111}, B_{111}, and C_{111} have been grown on Si(111) substrates, while samples labeled A_{110}, B_{110}, and C_{110} have been grown simultaneously on Si(110) substrates. For all samples, the growth has been performed on high-resistivity 3-in. silicon substrates ($\rho > 5\,k\Omega\,cm$) in order to provide a good transmission of THz waves by minimizing the free-carrier absorption. The two substrate orientations were chosen to probe the influence of the substrate on the far-IR transmission. One main advantage of the growth on Si(110) is the crystal lattice parameter matching between AlN and Silicon in the in-plane Si[001] direction, leading to a lower density of dislocations in the nucleation layer.[19]

The step-QW superlattices are deposited at 1050 °C on a stress mitigating stack to avoid cracks upon cooling. The growth rate of the GaN layers was 2 μm/h. The stack consists of a 20 nm thick AlN nucleation layer deposited at 1030 °C, a 200 nm thick AlN layer grown at 1150 °C, followed by two 500 nm thick GaN layers grown at 1050 °C separated by a 20 nm thick AlN layer grown at 930 °C. This stack induces a compressive strain in the following layers and then balances the tensile strain induced during cooling down, thus avoiding the formation of cracks. After growth, mirrorlike crack-free samples are obtained. AFM measurements have been performed on all samples in order to detect growth issues such as cracks or dislocations. These measurements reveal surfaces whose root-mean square (RMS) roughness is of the order of 0.7 nm, proving that the samples are of high quality. As an example, Fig. 1 shows the AFM surface ($10 \times 10\,\mu m^2$ scans) of samples A_{111} and A_{110}. The dislocation density is around $2 \times 10^9\,cm^{-2}$.

The samples were further characterized by high-resolution X-ray diffraction spectroscopy. Figure 2 shows ω-2θ scans around the (0002) X-ray reflection of the samples A–C grown on Si(111) and Si(110) substrates. As seen in Fig. 2, the satellite peaks originating from the active superlattice region have identical positions for samples A_{111} and A_{110} as well as for C_{111} and C_{110}. In turn, an increase in the superlattice period is observed for sample B_{110} with respect to B_{111}. Each spectrum has been simulated, using Epitaxy software (Panalytical), in order to extract the aluminum content and thicknesses of the different layers. The Al content is found to be close to the nominal values. However, the period and individual layer thicknesses are systematically slightly larger than the nominal values. Table I recasts the actual layer thicknesses. Additional characterizations were performed using SIMS in order to evaluate the Si doping concentration. The Si densities deduced from the SIMS measurements are mentioned in Table I.

Figures 3(a)–3(c) show the conduction-band profile and squared envelope functions for samples A, B, and C, respectively. Calculations were performed using the actual layer thicknesses deduced from X-ray spectroscopy, recapitulated in Table I using the Nextnano software.[20] The simulation relies on a self-consistent Schrödinger–Poisson solver accounting for the conduction-band nonparabolicity using the material parameters described in Ref. 21 and assuming periodic potential boundary conditions.[22] As seen in Fig. 3, the potential in the step barrier is almost flat except for a slight band bending due to the Coulomb interaction between electrons and ionized donors. The ground and excited electronic states are confined in the GaN well and $Al_{0.05}Ga_{0.95}N$ step barrier. This leads to large ISB dipole lengths of 4.1, 3, and 2.4 nm for samples A, B, and C, respectively. The bare e_1e_2 ISB transition energy without many-body corrections is predicted at 13.1 (3.1 THz), 17 (4.1 THz), and 26.9 meV (6.5 THz) for samples A, B, and C, respectively.

For transmission measurements, the samples were prepared as multipass waveguides whose length was chosen to allow two total internal reflections inside the waveguide. We then mechanically polished the two opposite facets of each piece at an angle of 45°. This angle was chosen to illuminate the input facet at normal incidence. Prior to mechanical polishing, a Ti(5 nm)/Au(200 nm) layer was deposited on the top surface (i.e., on the active regions). This configuration provides a good coupling of the TM-polarized terahertz radiation with the ISB transitions, thus enhancing the ISB absorption. Indium paste was used to glue the metallized surface on the cold finger of a liquid nitrogen-cooled cryostat. The transmission measurements were performed at 77 K using a Bruker Vertex 70 FTIR spectrometer equipped with a glow-bar source. Detection was provided by a liquid helium-cooled Si bolometer. A polarizer was placed in front of the sample. Pieces of bare silicon substrates with 45° angle polished facets and top surface metallization were used as a reference in order to normalize the measured transmission spectrum by the transmission of the substrate. The length of the reference samples was similar to that of the heterostructure samples.

TABLE I. Well, step, and barrier thicknesses deduced from XRD measurements, Si densities deduced from the SIMS measurements, and ISB transition energies deduced from Schrödinger-Poisson simulations without (E_{12}) and with (E_{12}^{depo}) the depolarization shift for samples A, B, and C grown on Si(111) and Si(110) substrates. The simulated values accounting for the depolarization shift are in good agreement with experiments (E_{12}^{exp}).

Sample	GaN thickness (nm)	$Al_{0.05}Ga_{0.95}N$ thickness (nm)	$Al_{0.1}Ga_{0.9}N$ thickness (nm)	Si doping in the well (cm^{-3})	E_{12} (meV)	E_{12}^{depo} (meV)	E_{12}^{exp} (meV)
A_{111}, A_{110}	3.6	17.6	3.5	7×10^{17}	13.1	21	23
B_{111}	3.3	11.0	3.3	1×10^{18}	17	28	29
B_{110}	3.6	11.9	3.6	1×10^{18}	16	27	28
C_{111}, C_{110}	3.5	8.6	3.4	7×10^{18}	26.9	41	37

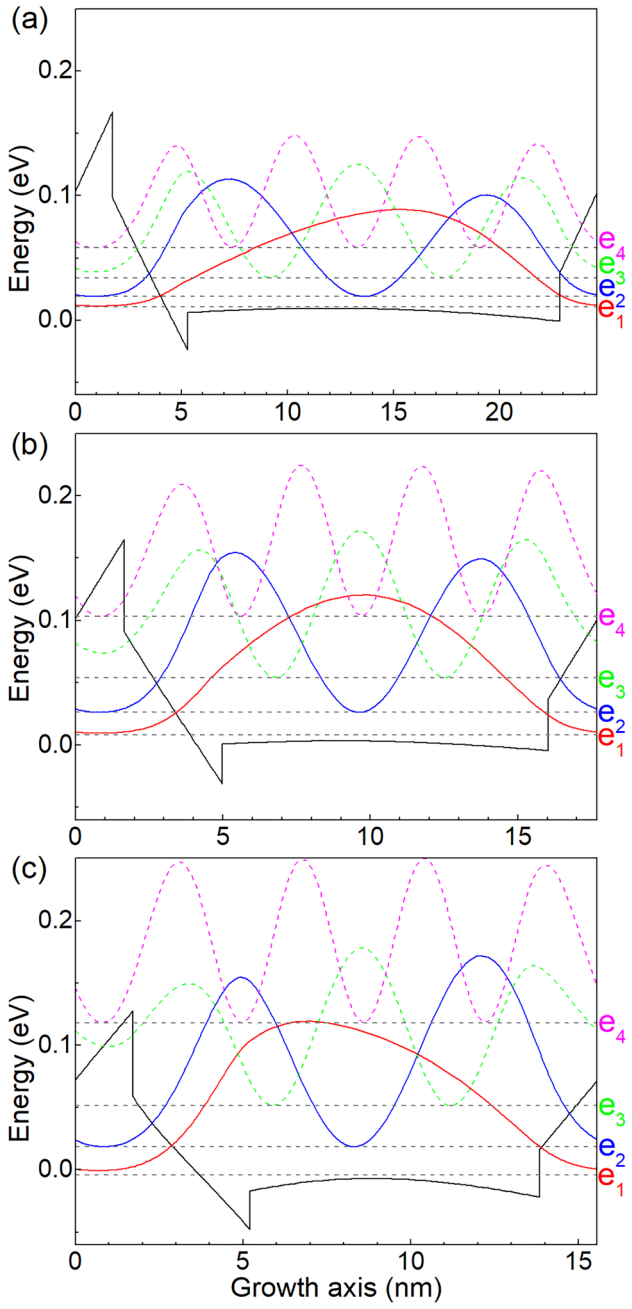

FIG. 3. Conduction-band profile and squared envelope functions of the bound electron states for samples A (a), B (b), and C (c).

Figures 4(a)–4(c) show the normalized TM/TE transmission spectra at 77 K of samples A_{111} and A_{110}, B_{111} and B_{110}, and C_{111} and C_{110}, respectively. The insets of Figs. 4(a)–4(c) present the transmission spectra for TE- and TM-polarizations of samples A_{110}, B_{111}, and C_{111}, respectively. As seen, all samples exhibit a TM-polarized absorption resonance. This is a clear proof of the ISB origin of the observed absorption. The ISB resonance is peaked at 23 meV (5.6 THz), 29 meV

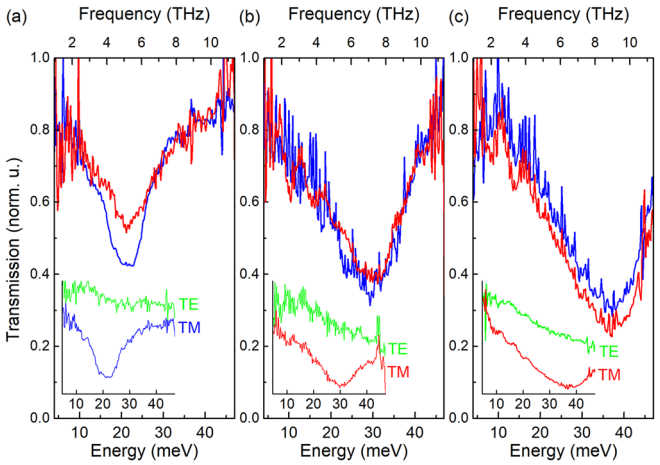

FIG. 4. Transmission spectra of samples A_{111} and A_{110} (a), B_{111} and B_{110} (b), and C_{111} and C_{110} (c) grown by MOVPE on Si(111) (red) and Si(110) (blue) substrates. The transmissions have been normalized by the transmission of the substrate for TM and TE-polarized light. The displayed spectra correspond to the TM/TE transmission ratio. The insets show the TM- and TE-polarized transmission spectra for samples A_{110} (a), B_{111} (b), and C_{111} (c), respectively.

(7 THz), and 37 meV (8.9 THz) for samples A, B, and C, respectively. It should be noted that the absorption magnitude and the peak energy are very close for samples grown on Si(111) and Si (110). The full width at half maximum (FWHM) of the ISB absorption is 11 meV (2.6 THz), 19 meV (4.7 THz), and 24 meV (5.8 THz) for samples A_{111}, B_{111}, and C_{111} and 12 meV (2.9 THz), 18 meV (4.4 THz), and 26 meV (6.2 THz) for samples A_{110}, B_{110}, and C_{110}, respectively. These values correspond to a broadening factor $\Delta E/E$ of 51%–54%, 60%–66%, and 65%–69% for samples A, B, and C, respectively. Nextnano simulations show that this rather large broadening cannot be attributed to the fluctuations of the layer thickness. The dispersion of the e_1e_2 ISB transition energy accounting for a ± 1 monolayer fluctuation of each layer does not exceed 2.6 meV for all samples, the value of which is much smaller than the experimental FWHM. In addition, the fact that the FWHM gets broader from the lowest doped sample A to the highest doped sample C indicates that the main contributions to the broadening are the electron-impurity and electron-electron scatterings in agreement with published work.[11,15] However, one cannot exclude at this stage some extra broadening arising from ISB transitions from the e_2 state to higher excited states, provided that the e_2 state is populated.

We have estimated the effective electron concentration and the Fermi energy in the wells based on the measured ISB absorbance (the method is described in Ref. 23). The peak absorbance deduced from the transmission measurements of Fig. 4 is 0.29, 0.35, and 0.46 (0.19, 0.4, and 0.52) for samples A, B, and C grown on Si(111) [Si(110)]. Based on the calculated dipole length and the experimental transition energy and broadening, the 2D electron concentration between the e_1 and e_2 subbands, n_1-n_2, can be estimated (accounting for a 51.8° refraction angle in the active layers). For samples A, B, and C grown on Si(111) [on Si(110)], n_1-n_2 is deduced to be $\sim 2.6 \times 10^{11}$, 7.6×10^{11}, 1.5×10^{12} (1.9×10^{11}, 7.6×10^{11}, 1.8×10^{12}) cm^{-2}, respectively. The deduced volumetric electron concentrations are close to the values estimated from the SIMS measurements. Based on these values,

we estimate that the Fermi energy at 77 K with respect to the e_1 ground state energy is around −4, 5.5, and 16 meV for samples A, B, and C, respectively. This means that the population of the e_2 state is negligible at 77 K and that only e_1e_2 ISB transitions contribute to the observed absorptions.

In the THz spectral range, one cannot neglect the effect of many-body interactions such as the depolarization shift, which arises from the screening of the ISB resonance by the electron plasmons. We have estimated the depolarization shift of the ISB absorption induced by the electron concentration in the step-QWs following the perturbation treatment of Refs. 24 and 25. The correction amounts to more than 50% of the ISB energy calculated in a single particle approximation. Table I recasts the sample parameters deduced from the structural characterizations and Si doping estimations as well as the measured and calculated ISB transition energies accounting for the depolarization shift. As seen, there is excellent agreement between measurements and simulations when the depolarization shift is taken into account.

In conclusion, we have reported the observation of the ISB absorption at terahertz frequencies in GaN/AlGaN step-QWs grown by MOVPE on both Si(111) and Si(110) substrates. The sample design targets a flatband potential in the wells to allow for an ISB absorption in the terahertz frequency range and to improve the optical dipole moments. The rather large broadening of the ISB absorption, in the range of 50%–66%, is attributed to electron-impurity and electron-electron scattering due to the rather large carrier concentrations. The observed ISB absorption energies are in good agreement with simulations accounting for the depolarization shift induced by the electron concentration.

The authors acknowledge support from the French ANR program “OptoTeraGaN” and Labex GaneX.

REFERENCES

[1]R. Köhler, A. Tredicucci, F. Beltram, H. E. Beere, E. H. Linfield, A. G. Davies, D. A. Ritchie, R. C. Iotti, and F. Rossi, Nature **417**, 156 (2002).
[2]B. S. Williams, S. Kumar, Q. Hu, and J. L. Reno, Opt. Express **13**, 3331 (2005); B. S. Williams, S. Kumar, Q. Qin, Q. Hu, and J. L. Reno, Appl. Phys. Lett. **88**, 261101 (2006); B. S. Williams, Nat. Photonics **1**, 517 (2007).
[3]C. Walther, M. Fischer, G. Scalari, R. Terazzi, N. Hoyler, and J. Faist, Appl. Phys. Lett. **91**, 131122 (2007).
[4]H. Luo, S. R. Laframboise, Z. R. Wasilewski, G. C. Aers, H. C. Liu, and J. C. Cao, Appl. Phys. Lett. **90**, 041112 (2007).
[5]V. D. Jovanović, D. Indjin, Z. Ikonić, and P. Harrison, Appl. Phys. Lett. **84**, 2995 (2004).
[6]E. Bellotti, K. Driscoll, T. D. Moustatkas, and R. Paiella, Appl. Phys. Lett. **92**, 101112 (2008).
[7]E. Bellotti, K. Driscoll, T. D. Moustatkas, and R. Paiella, J. Appl. Phys. **105**, 113103 (2009).
[8]L. Bosco, M. Franckié, G. Scalari, M. Beck, A. Wacker, and J. Faist, Appl. Phys. Lett. **115**, 010601 (2019).
[9]M. Wienold, B. Röben, L. Schrottke, R. Sharma, A. Tahraoui, K. Biermann, and H. T. Grahn, Opt. Express **22**, 3334 (2014).
[10]M. Tchernycheva, L. Nevou, L. Doyennette, F. H. Julien, E. Warde, F. Guillot, E. Monroy, E. Bellet-Amalric, T. Remmele, and M. Albrecht, Phys. Rev. B **73**, 125347 (2006).
[11]P. K. Kandaswamy, H. Machhadani, C. Bougerol, F. H. Julien, and E. Monroy, Appl. Phys. Lett. **95**, 141911 (2009).
[12]H. Durmaz, D. Nothern, G. Brummer, T. D. Moustakas, and R. Paiella, Appl. Phys. Lett. **108**, 201102 (2016).
[13]C. B. Lim, A. Ajay, C. Bougerol, B. Haas, J. Schoermann, M. Beeler, J. Laehnemann, M. Eickhoff, and E. Monroy, Nanotechnology **26**, 435201 (2015).
[14]H. Machhadani, M. Tchernycheva, S. Sakr, L. Rigutti, R. Colombelli, E. Warde, C. Mietze, D. J. As, and F. H. Julien, Phys. Rev. B **83**, 075313 (2011).
[15]C. B. Lim, A. Ajay, C. Bougerol, J. Lähnemann, F. Donatini, J. Schörmann, E. Bellet-Amalric, D. A. Browne, M. Jiménez-Rodriguez, and E. Monroy, Nanotechnology **27**, 145201 (2016).
[16]F. F. Sudradjat, W. Zhang, J. Woodward, H. Durmaz, T. D. Moustakas, and R. Paiella, Appl. Phys. Lett. **100**, 241113 (2012).
[17]M. Beeler, C. Bougerol, E. Bellet-Amalric, and E. Monroy, Appl. Phys. Lett. **105**, 131106 (2014).
[18]W. Terashima and H. Hirayama, Phys. Status Solidi C **8**, 2302 (2011).
[19]Y. Cordier, J.-C. Moreno, N. Baron, E. Frayssinet, J.-M. Chauveau, M. Nemoz, S. Chenot, B. Damilano, and F. Semond, J. Cryst. Growth **312**(19), 2683–2688 (2010).
[20]See http://www.nextnano.de for “Nextnano3 Software.”
[21]I. Vurgaftman and J. R. Meyer, J. Appl. Phys. **94**, 3675 (2003).
[22]H. Machhadani, P. Kandaswamy, S. Sakr, A. Vardi, A. Wirtmüller, L. Nevou, F. Guillot, G. Pozzovivo, M. Tchernycheva, A. Lupu, L. Vivien, P. Crozat, E. Warde, C. Bougerol, S. Schacham, G. Strasser, G. Bahir, E. Monroy, and F. H. Julien, New J. Phys. **11**, 125023 (2009).
[23]M. Helm, in *Intersubband Transitions in Quantum Wells: Physics and Device Applications I*, edited by H. C. Liu and F. Capasso (Academic, New York, 2000).
[24]K. M. S. V. Bandara, D. D. Coon, O. Byungsung, Y. F. Lin, and M. H. Francombe, Appl. Phys. Lett. **53**, 1931 (1988).
[25]K. M. S. V. Bandara, D. D. Coon, O. Byungsung, Y. F. Lin, and M. H. Francombe, Appl. Phys. Lett. **55**, 206 (1989).